Journal of Materials Chemistry C

Chlorine-Mediated Atomic Layer Deposition of HfO2 on Graphene

Journal:	*Journal of Materials Chemistry C*
Manuscript ID	TC-ART-07-2021-003502.R2
Article Type:	Paper
Date Submitted by the Author:	17-Nov-2021
Complete List of Authors:	Wilson, Peter; Army Research Laboratory, Sensors and Electron Devices Directorate Chin, Matthew; Army Research Laboratory Ekuma, Chinedu; Lehigh University, Physics; Lehigh University, Institute for Functional Materials and Devices Najmaei, sina; US Army Research Laboratory, Price, Kate ; Army Research Laboratory, Sensors and Electron Devices Directorate Schiros, Theanne; Columbia University, Materials Research Science and Engineering (MRSEC) Dubey, Madan; Army Research Laboratory, Sensors and Electron Devices Directorate Hone, James; Columbia University

Chlorine-Mediated Atomic Layer Deposition of HfO_2 on Graphene

Peter M. Wilson,[1] Matt L. Chin,[1] Chinedu E. Ekuma,[2,3] Sina Najmaei,[1] Katherine M. Price,[1] Theanne Schiros,[5,6] Madan Dubey,[1] James Hone[4]

[1] Sensors and Electron Devices Directorate, United States Army Research Laboratory, Adelphi, MD, USA

[2] Department of Physics, Lehigh University, Bethlehem, PA, 18015 USA

[3] Institute for Functional Materials and Devices, Lehigh University, Bethlehem, PA, 18015 USA

[4] Department of Mechanical Engineering, Columbia University, New York, New York 10027, United States

[5] Materials Science and Engineering Center, Columbia University, New York, NY 10023

[6] Department of Science and Mathematics, Fashion Institute of Technology, New York, NY 10001

Abstract

Although graphene and other 2D materials have been extensively studied with superlative electrical properties already reported, several processing constraints impede integration into advanced device structures. One such constraint is the chemical inertness of graphene, which has hindered the deposition of thin high-κ dielectrics, e.g., HfO_2 by processes such as the atomic layer deposition (ALD) technique. Through computational-guided experiments, we demonstrate that a partially defective chlorine adlayer on a graphene surface significantly improves the nucleation of HfO_2. The evolution of chlorinated graphene (CG) during the deposition of HfO_2 via ALD was monitored with Raman spectroscopy and X-ray photoelectron spectroscopy (XPS), and modeled using first-principles calculations. Our calculations show that the enhancement of the ALD of HfO_2 is due to chlorine vacancies in the chlorine adlayer, which act as nucleation sites for HfO_2. Our experiment supports this observation; some thermally activated chlorine molecules partially desorbed from the graphene surface during the ALD process. This process enabled the deposition of a conformal 3.5 nm HfO_2 layer on graphene, which resulted in top-gated field-effect transistors (FETs) with no gate-leakage and hysteresis of less than 10 mV. Our work demonstrates a scalable and reliable approach for the integration of ultra-thin high-κ dielectrics onto graphene-based devices.

Introduction

Since the successful synthesis and characterization of graphene in 2004, much attention has been devoted to exploring and exploiting graphene's superlative electrical properties.[1] Proposed applications of graphene abound, ranging from high-performance field-effect transistors (FETs)[2,3], flexible electronics[4,5], and

sensors.[6–8] However, harnessing, implementing, and integrating graphene technologies remain a challenge due to the numerous processing constraints inherent with graphene. Atomic layer deposition (ALD) of metal oxide dielectrics is one of the most promising routes toward integrating graphene with other material systems. Additionally, ALD is a standard technique in industrial applications and offers self-limiting layer-by-layer thickness control, controllable kinetic process conditions, and high conformality. However, high quality ALD of metal oxide dielectrics on graphene has proven to be challenging.[9] This is due to graphene's chemically inert surface. The ALD process is chemically facilitated by adsorption and the reaction of the metal-organic precursor to a chemically reactive surface, which graphene does not possess. As a result, nucleation of metal oxide dielectrics on the graphene surface via ALD tends to be highly polydisperse, which results in poor coverage of metal oxides at low thicknesses and requires dozens of nanometers to attain full coverage.[9]

Current ALD processes can circumvent the problem of graphene's chemical inertness by "seeding" the graphene with a monodisperse coating of chemical species, such as metals[10–12] or perylene tetracarboxylic acid[13,14] that act as nucleation sites. While this improves the growth of the metal oxide film, it compromises the interface and dielectric integrity. Other methods, such as partial oxidation of the graphene surface via ozone or remote oxygen plasma, have also led to increased chemical activity. This process generates oxygen functional groups on the graphene to act as nucleation sites, but also reduces the quality of the graphene by introducing defects, which strongly scatter carriers.[15,16]

Recently, the chemical and electrical properties of chlorinated graphene (CG) have attracted a lot of research interest.[17,18] Previous reports have shown that photochlorinated graphene results in covalent bonding between chlorine and carbon[19,20], strongly diminishing the electrical properties of graphene. Meanwhile, plasma functionalization of graphene has been shown to result in a more stable configuration of chlorographene via the chemisorption of chlorine on the graphene surface.[18] In this configuration, the chemisorption of chlorine on graphene is stabilized by the removal of electron charge from the graphene and the resulting charge redistribution within the plane of the adlayer of chlorine.[21] More importantly, the

chemisorbed chlorine does not covalently bind to the surface of graphene; hence does not disrupt the sp^2 hybridization of graphene despite attaining a high stoichiometric ratio of chlorine to carbon of ~ 50%.[18]

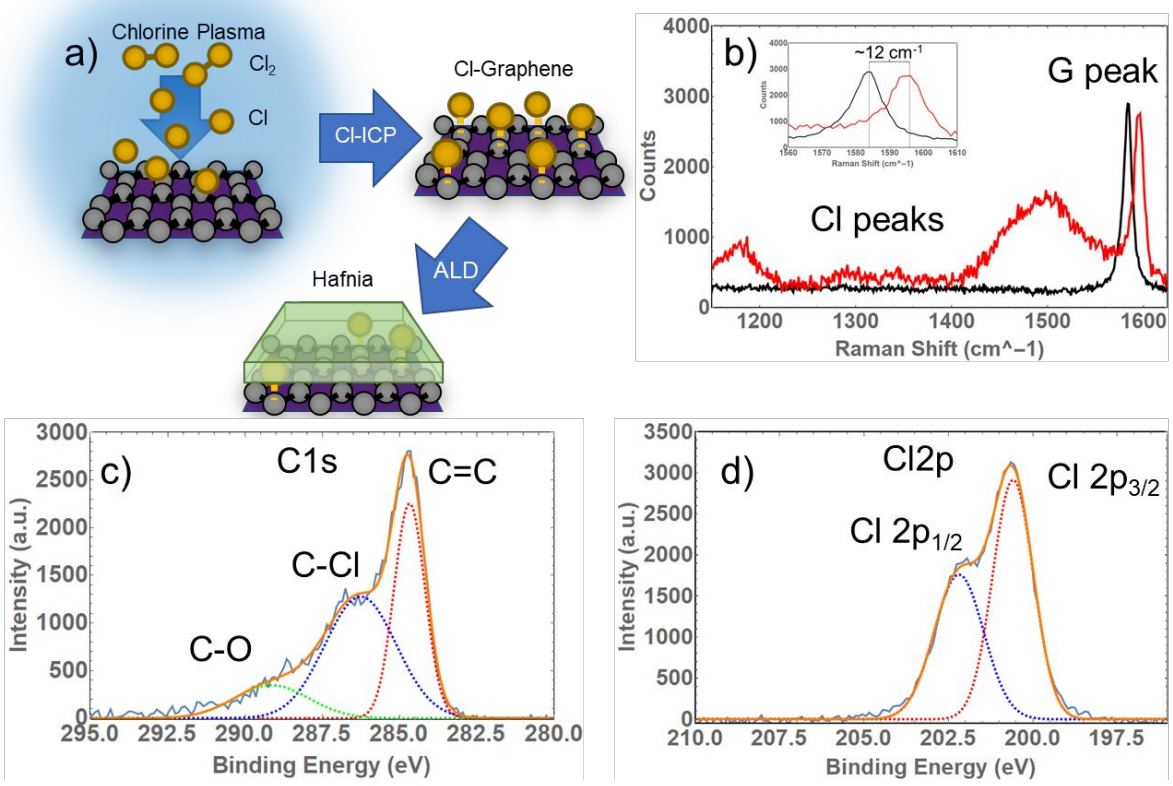

Figure 1: Schematic of chlorine-mediated ALD process (a). Raman spectra both before (black) and after (red) chlorination of the graphene. The emergence of new peaks around 1150 and 1500 1/cm coincide with chlorine on the graphene surface. The inset shows the Raman G peak shift of ~12 cm^{-1} indicative of doping. (b). XPS spectra of the C-*1s* (c) and Cl-*2p* (d) region corresponding to a Cl:C ratio of ~47%.

Motivated by this promising stability of chlorine-functionalized graphene, we explore the ALD growth of HfO_2 high-κ dielectrics on chlorinated graphene and explore whether the chlorine adlayer could be engineered to increase the nucleation of metal oxide growth. We investigate whether chlorine mediates the deposition of HfO_2 as shown schematically in Figure 1a. The chemical adsorption of the HfO_2 precursors to graphene and CG surfaces is monitored by XPS and Raman spectroscopy, and modeled via first-principles calculations. Combining experiments and first-principles simulations, we demonstrate that the ALD growth of HfO_2 is aided by the presence of chlorine adsorbates on graphene's basal plane. Back-gated

FETs of CG were designed and used to probe the quality of the device performance pre- and post-ALD. Finally, a top-gated CG device was fabricated with an ultra-thin ALD HfO_2 gate dielectric of ~ 3.5 nm.

Methods

Material Processing. Graphene was isolated using scotch tape-assisted mechanical exfoliation onto heavily p-doped Si with a 285 nm SiO_2 thermally-grown layer. The samples were chlorinated via chlorine plasma using an Oxford PlasmaLab 100 at 75 mTorr, 20 sccm Cl_2, 200W ICP power, 10W RF power, and 22 ^oC for 15 seconds. This resulted in an accelerating bias of ~3V during the plasma treatment. Chlorine coverage on the samples was modulated by thermally removing chlorine via heating at 120 °C for 8 hours before subsequent XPS and then immediate ALD. For samples requiring a high chlorine content during the ALD process, ALD was performed on the samples within 24 hours following immediate XPS measurement.

ALD was conducted using a Kurt J. Lesker ALD-150LX deposition system at 120 ^oC with the following step times: 0.25 s pulse Tetrakis(dimethylamido)hafnium (IV) (TDMAH) precursor/ 15 s purge/ 0.4 s pulse oxidant/ 15 s purge.

Characterization. Raman measurements were taken using a Renishaw InVia Raman microscope with a 532 nm laser. XPS spectra were taken using a PHI Versaprobe II with an aluminum 1486 eV x-ray source. AFM measurements were taken using a Bruker Nanoscope V atomic force microscope.

Device Preparation. Field-effect transistors based on the HfO_2-coated chlorinated graphene were designed and fabricated to determine the electrical properties of the treated graphene. Graphene was exfoliated onto 285 nm of thermally oxidized SiO_2 on Si substrates. The chlorinated graphene transistors possessed channel widths of 1 μm and channel lengths of 2 μm. The source-drain contacts were composed of 10/85 nm of Ti/Au deposited via e-beam evaporation, and the ALD-based HfO_2 dielectric was deposited with a nominal thickness of 3.5 nm (30 cycles). I-V measurements were performed to determine the effect of chlorination on the electrical properties of the graphene field-effect transistor, including the Dirac point, the channel conductance, carrier type, and field-effect mobility.

Computational Method. First-principles calculations were performed using density functional theory (DFT)[22,23] with a planewave basis set as implemented in the *VASP* code.[24] The calculations were carried out using the Perdew-Burke-Ernzerhof exchange-correlation functional.[25] The energetics of the graphene-chlorine composite, i.e., CG is designed with a $6 \times 6 \times 1$ graphene slab (72 atoms) with the chlorine (18 atoms) corresponding to 25% coverage. The Cl atoms are positioned such that the formation of Cl molecules, which leads to desorption from the graphene surface, is prohibited. At equilibrium configuration, the chlorine forms a hexagonal structure sitting at ~ 1.91 Å above the graphene plane with an average Cl-Cl bond length of ~ 2.84 Å, which is significantly greater than the ~ 1.77 Å Cl-Cl bond length of the Cl molecule. The adsorption of the synthetic Cl crystal on the graphene slab induced a small buckling to the graphene plane, with the C-C bond length decreasing to ~ 1.40 Å. There are numerous potential orientations of the adsorption of the TDMAH precursor on the CG. To determine the most energetically favorable orientation of the precursor, we used the nudged elastic band method.[26] In all the calculations, we employed an $8 \times 8 \times 1$ Γ-centered grid to sample the reciprocal space with a kinetic energy cutoff of 550 eV and a vacuum size of ~ 20 Å to separate periodic images. During relaxation, the ionic positions were allowed to move while keeping the volume of the cell constant. The hybrid structures were fully relaxed until the energy (charge) converged to within ~10^{-3} (10^{-7}) eV and the forces dropped to ~10^{-3} eV/Å. All calculations included van der Waals interactions.

Results and Discussion

Chlorine treatment of graphene resulted in a ~50% coverage of the full graphene monolayer surface (defined as a Cl:C ratio of 0.5) as determined by integrating the intensities of the XPS C-*1s* and Cl-*2p* peaks (Figure 1c, d) and normalizing by the corresponding photoionization cross-section. The presence of chlorine on the graphene results in the emergence of Raman peaks around 1100, 1300, and 1500 cm^{-1} (Figure 1b).

The emergence of these peaks is a unique feature of chlorine on graphene (Figure S1) as they appear on chlorinated graphene and not on SiO_2; details of this will be addressed in a forthcoming paper. Upon adsorption of the chlorine, the graphene becomes significantly *p*-doped due to chlorine's high electronegativity compared with carbon, as evidenced spectroscopically by the shift in the G peak by ~12 cm^{-1}.[27,28] However, despite the high coverage of chlorine on the surface of graphene, no D band formation is observed in the Raman spectra, suggesting that the plasma treatment and chlorine adsorption does not induce significant defect states in the graphene, thereby preserving its electrical properties. This observation is in agreement with previous studies.[17,18]

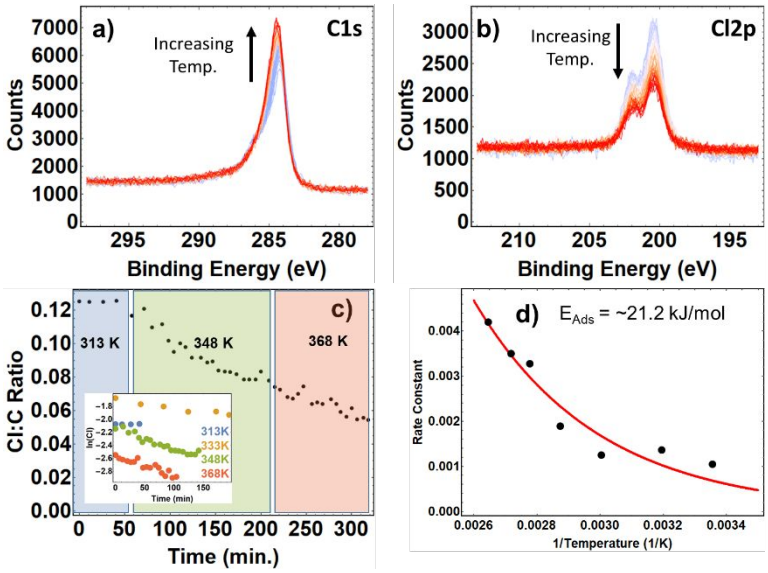

Figure 2: XPS temperature-programmed desorption data. a) C-*1s* region of the spectrum showing increasing carbon sp^2 peak intensity with increasing temperature. b) Cl-*2p* region of the spectrum showing loss of chlorine intensity with increasing temperature. c) Cl:C ratio vs. time for three different temperature regimes. Inset: log plot of chlorine loss over time. d) Arrhenius plot of chlorine desorption showing adsorption energy of 21.2 kJ/mol.

The non-covalent nature of the Cl-graphene interaction is supported by temperature-dependent XPS probed desorption measurements of the chlorinated graphene films. Figures 2a and 2b show the C-*1s* and Cl-*2p* area of the XPS spectrum, respectively. As the temperature increases, the chlorine content decreases dramatically while the carbon signal rises slightly. This observation correlates well with the loss of physisorbed chlorine. The slight increase in the C-*1s* spectrum is consistent with the removal of non-carbon adatoms from the surface. In Figure 2c, we present the change in the Cl:C ratio over time at different

temperatures (inset is the log plot). Note that the Cl:C ratio is essentially constant up to 313 K. This signifies that the X-ray irradiation alone is not sufficient to remove chlorine from the graphene surface. The Arrhenius plot (Figure 2d) enables an estimate of the adsorption energy of the chlorine to the graphene surface, which is ~ 21.2 kJ/mol. This is within the order of magnitude indicative of chemisorption rather than a covalent bond.

To investigate the effect of chlorine coverage on ALD growth, three sample sets were prepared: pristine exfoliated graphene, lightly chlorinated graphene (LCG) with a chlorine coverage of ~17%, and heavily chlorinated graphene (HCG) with a chlorine coverage of ~53%. The evolution of the ALD HfO_2 with chlorine coverage is demonstrated by the array of atomic force microscopy (AFM) images (Figure 3a-h). We explored the impact of chlorine coverage in the early stages of ALD by halting the deposition process after 16 cycles with a nominal film thickness of 2 nm. HfO_2 coverage was computed by normalizing the HfO_2-covered regions using the total image dimensions of the AFM images (Figure S2) and the chlorine coverage was obtained from the XPS. The data are summarized in Figure 3j. After 16 cycles, the deposition on bare graphene is highly irregular with very low coverage of ~29.4% as determined by taking the ratio of HfO_2-covered regions with total image dimensions from phase-image AFM. The coverage after 16 cycles increases for the LCG sample with total HfO_2 coverage of ~36.0%. We observe that the coverage continued to increase for the HCG sample reaching total coverage of ~61.6%, which strongly suggests that the presence of chlorine on the graphene surface enhances the nucleation rate of ALD HfO_2.

For thicker HfO_2 layers, improved nucleation was observed for CG resulting in more conformal ALD HfO_2 with reduced roughness. The deposition of 5 nm HfO_2 on pristine graphene led to a highly polydisperse coating of HfO_2 nanoparticles, with a high roughness of ~2.27 nm and still not attaining full coverage. In the LCG sample, the 5 nm growth formed a nearly conformal coating of HfO_2 with a roughness of ~0.895 nm. Coverage was drastically improved on the HCG, with ALD coverage reaching 100% and with a rather low roughness of ~0.283 nm. We observed continuous improvement on the coverage with higher Cl concentration for thicker samples ~10 nm deposition with 80 cycles. We note that the 10 nm deposition on

the pristine graphene was still not conformal, with cracks in the HfO_2 and surface roughness of ~1.99 nm. Conformal coatings were obtained on the LCG and HCG samples using the same process with the roughness decreasing with increasing chlorine coverage. These results strongly suggest that chlorine on the graphene surface greatly assists the ALD process by providing a high density of nucleation sites.

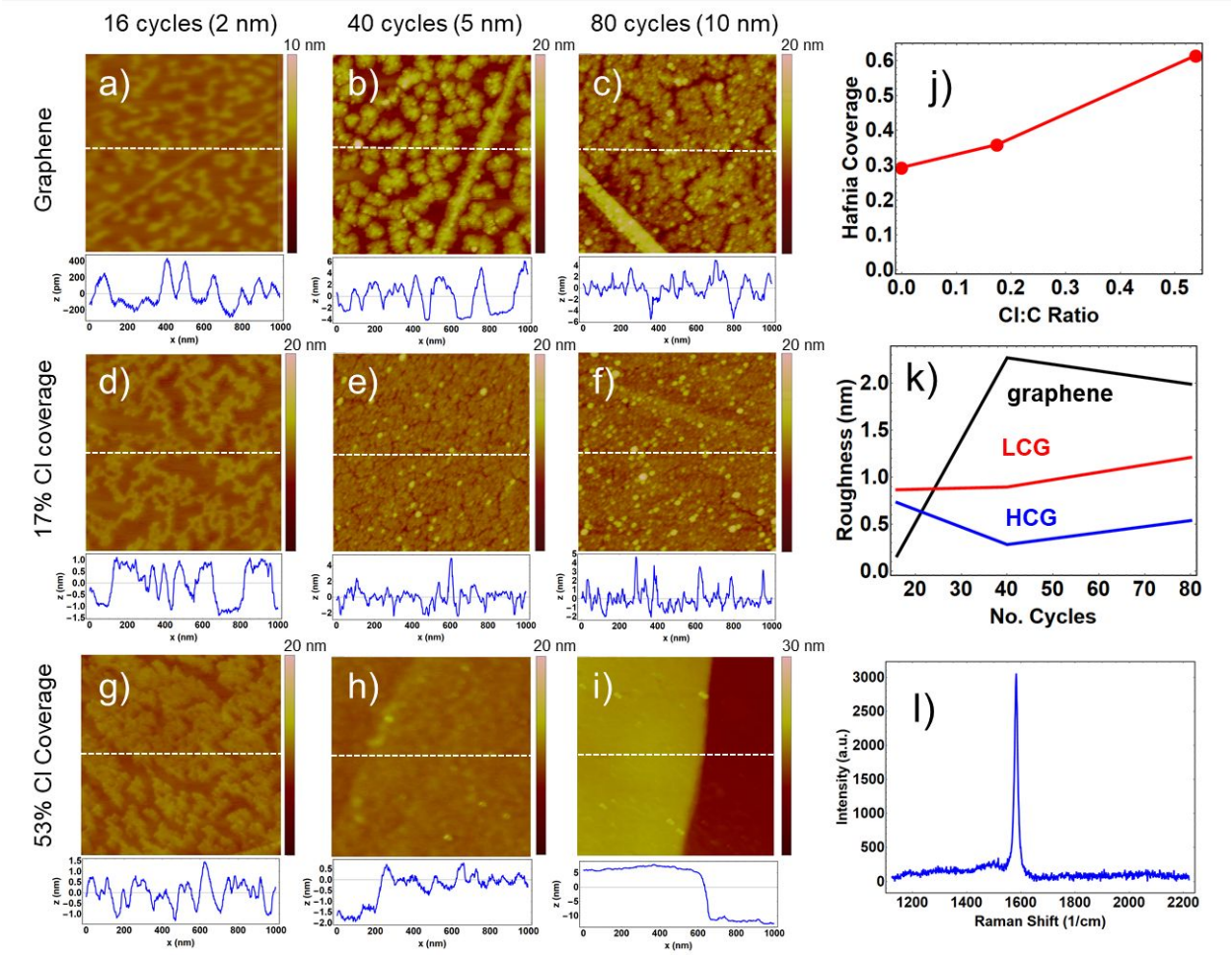

Figure 3: AFM images of pristine graphene with 2 (a), 5 (b), and 10 nm (c) of HfO_2 deposited by ALD and of LCG with 2 (d), 5 (e), and 10 nm (f) of HfO_2 and on the deposition of HCG of 2 (g), 5 (h), and 10 nm (i) of HfO_2. Line scans are shown below the corresponding AFM image. HfO_2 coverage as a function of Cl:C ratio on graphene surface following 16 cycles of ALD growth nominally resulting in ~2nm of HfO_2 (j). Evolution of the roughness profiles of graphene, LCG, and HCG with increasing ALD cycles (k). Raman spectrum of CG post-ALD showing a decrease in Cl peaks around 1150 and 1500 1/cm suggesting a decrease in Cl:C ratio to <10% (l).

To gain deeper insights into the impact of chlorinating graphene, we measured the Raman spectra. Our data confirm the presence of remnant chlorine as evidenced by the persistence of the peak structure around 1500 cm^{-1} (Figure 3l). However, the Cl peaks appear significantly diminished compared to the uncoated Cl-

graphene sample, suggesting that some chlorine had desorbed in the process. Estimates of the Cl concentration based on the Raman spectra suggest a chlorine coverage of <10% (Cl:C < 0.10) based on the Cl peak/G ratio (Figure S3). The chlorine was likely desorbed from the graphene by two routes. Firstly, it will have desorbed in the form of a chlorine molecule as a result of the increased temperature during the ALD process; this is supported by the temperature probe desorption data presented in Figure 2. Secondly, since chlorine is in a reactive state while adsorbed to the graphene surface, the chlorine will have reacted with the hafnium upon TDMAH exposure. This could be inferred from the Cl-2p peak in the XPS (Figure S4), which redshifted to ~198 eV after the deposition of 2 nm of hafnia, consistent with the inorganic chlorine peak. It should be noted that due to the overcoating layer of hafnia, the XPS is not well suited for quantitative characterization of sublayers of graphene or chlorine beneath the hafnia and is only somewhat useful after a few ALD cycles.

The interplay between chlorine coverage, the thermal desorption of chlorine, and uniform HfO_2 growth motivates investigation into the mechanism of HfO_2 growth. Most significantly, we need to discern the potential role defects in the chlorine adlayer play in the HfO_2 deposition. To explore this, we use first-principles modeling based on the density functional theory calculations to probe the nucleation mechanisms in the CG. We can gain some understanding of this process by examining the energetics of the overall adsorption process. The adsorption energy is a vital parameter in this regard. To this end, we computed the adsorption energy (E_{ads}) at various experimental settings. The E_{ads} of TDMAH on pristine graphene is computed to be ~ -0.49 eV (Figure 4a). Using a chlorine coverage of 25% on the graphene surface, we obtain $E_{ads} \sim$ -0.51 eV. The negligible decrease (~0.02 eV) in the adsorption energy does not sufficiently account for the dramatic improvement in the nucleation that we observed in the experiment. To adequately address this, we carried out a series of calculations with Cl vacancies in the CG superstructure. We observed that Cl vacancies significantly decreased the adsorption energy, e.g., removing half of the Cl atoms led to $E_{ads} \sim$ -0.79 eV, a substantial decrease of $\sim$ 0.28 eV. Therefore, it appears that vacancies in the chlorine adlayer are primarily responsible for the improved nucleation of HfO_2 on the CG surface.

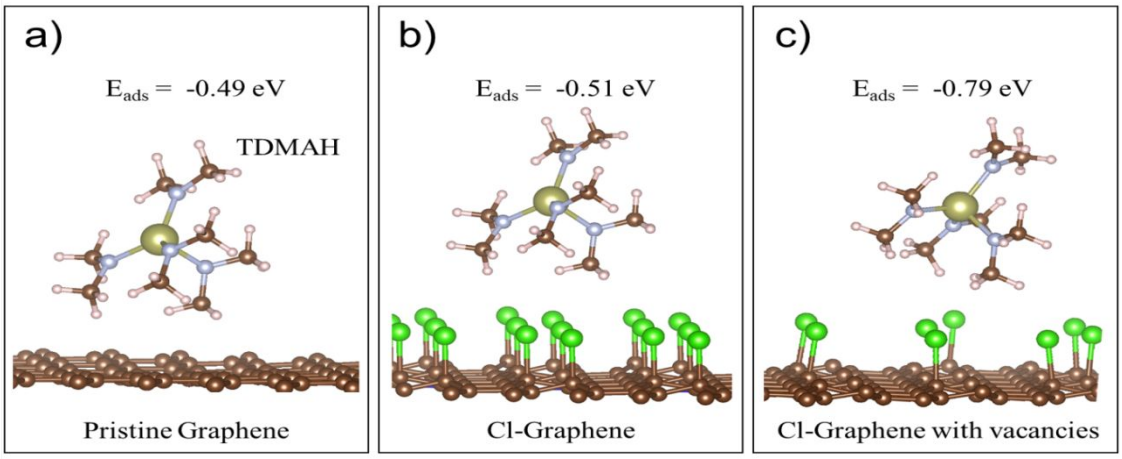

Figure 4: Optimized superstructure of a TDMAH molecule on (a) graphene, (b) CG, and (c) CG with Cl vacancies including their corresponding adsorption energy, E_{ads}.

On CG with a high initial Cl:C ratio, a conformal and smooth HfO_2 layer should be achievable at ~3.5 nm. To investigate this, graphene FETs were fabricated and chlorinated as before. HfO_2 was deposited with a 30-cycle run, resulting in a layer approximately 3.5 nm thick. The back-gated transfer properties of the device were measured at each step in the process, and finally, a top gate was added and measured. The transfer properties for the back-gated measurements are presented in Figure 5a. We observe that the chlorination of graphene significantly shifts the charge neutrality point from +7 V (nominally indicating *p*-type doping) to +53 V with a hole doping concentration of ~3.5 X 10^{12} cm^{-2}, which is consistent with the Raman spectra. The charge neutrality point shifts downward to +41 V after depositing the HfO_2 dielectric, indicating a reduction in the hole-dominated transport. This is consistent with the desorption of Cl during the ALD process.

Top-gated current-voltage (I-V) transfer properties were measured following the deposition of Ti/Au top-gate structures (inset Figure 5b) on the device channels. The corresponding transfer curve is shown in Figure 5b. The device exhibits a charge neutrality point at ~0.1 V, which implies a slight *p*-doping of the graphene channel. Importantly, the device exhibited no gate leakage with negligible leakage current; suggesting that the deposition of ~3.5 nm HfO_2 resulted in a conformal and uniform dielectric on the graphene surface,

making the device suitable for top gating. Furthermore, within the voltage range probed in the device set, hysteresis was minimal, indicative of the absence of charge traps and uniform dielectric growth.

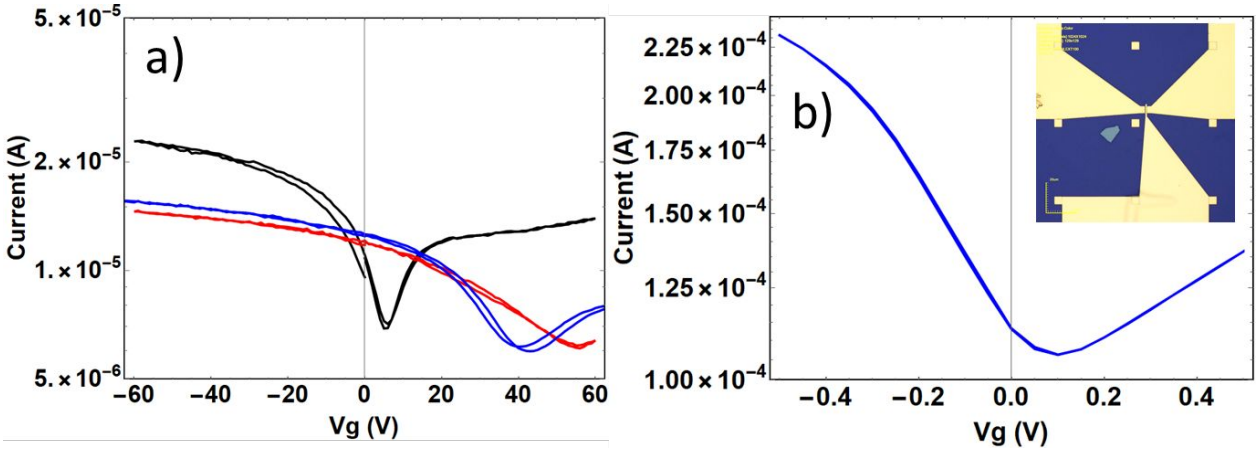

Figure 5: Various electrical measurements were used to characterize a graphene transistor device, with back-gated I-V measurements (a) for the device when it possessed a pristine graphene channel (black) after it was chlorinated (red), and after ALD HfO2 was deposited on top of the chlorinated graphene (blue). Top-gated measurements taken after a 3-nm thick HfO2 layer was deposited are represented in (b), and a micrograph of the complete graphene transistor structure is shown in (inset (b)).

In conclusion, chlorine adsorbates on the surface of graphene are found to assist in the conformal ALD of HfO_2 by increasing the nucleation density. Our data and the analysis suggest that the ALD process led to the partial removal of chlorine as thermally activated chlorine molecules, which resulted in the formation of defect sites in the chlorine adlayer. These defective sites in turn act as nucleation sites for the adsorption of TDMAH molecule, which significantly decreased the adsorption energy compared with both the pristine graphene and the fully chlorinated CG samples. Our approach demonstrates a potential route to deposit a conformal, ultrathin layer ~3.5 nm thick of HfO_2, which is sufficient for use as a top-gate dielectric. The resulting multilayer graphene devices exhibited slight *p*-transport with the absence of gate-leakage and minimal hysteresis. This could pave the way for easier integration of graphene and possibly, other 2D materials into electronic devices.

Acknowledgments

The research was sponsored by the Army Research Laboratory and was accomplished under Cooperative Agreement Number W911NF-18-2-0028. Additionally, this work was supported in part by the NSF MRSEC program through the Center for Precision Assembly of Superstratic and Superatomic Solids, Columbia University (DMR-1420634), and a startup grant from Lehigh University. Computational resources were provided by the DOD High-Performance Computing Modernization Program at the Army Engineer Research and Development Center, Vicksburg, MS. The views and conclusions contained in this document are those of the authors and should not be interpreted as representing the official policies, either expressed or implied, of the Army Research Laboratory or the U.S. Government. The U.S. Government is authorized to reproduce and distribute reprints for Government purposes notwithstanding any copyright notation herein.

References

(1) Novoselov, K. S.; Geim, A. K.; Morozov, S. V; Jiang, D.; Zhang, Y.; Dubonos, S. V; Grigorieva, I. V; Firsov, A. A. Electric Field Effect in Atomically Thin Carbon Films. *Science* **2004**, *306* (5696), 666–669. https://doi.org/10.1126/science.1102896.

(2) Schwierz, F. Graphene Transistors. *Nat. Nanotechnol.* **2010**, *5* (7), 487–496. https://doi.org/10.1038/nnano.2010.89.

(3) Farmer, D. B.; Xia, F.; Jenkins, K. A.; Bol, A. A.; Lin, Y.; Zhu, Y.; Wu, Y.; Avouris, P. High-Frequency, Scaled Graphene Transistors on Diamond-like Carbon. *Nature* **2011**, *472* (7341), 74–78. https://doi.org/10.1038/nature09979.

(4) Jang, H.; Park, Y. J.; Chen, X.; Das, T.; Kim, M. S.; Ahn, J. H. Graphene-Based Flexible and Stretchable Electronics. *Adv. Mater.* **2016**, *28* (22), 4184–4202. https://doi.org/10.1002/adma.201504245.

(5) Kim, B. J.; Jang, H.; Lee, S. K.; Hong, B. H.; Ahn, J. H.; Cho, J. H. High-Performance Flexible Graphene Field Effect Transistors with Ion Gel Gate Dielectrics. *Nano Lett.* **2010**, *10* (9), 3464–

3466. https://doi.org/10.1021/nl101559n.

(6) Hill, E. W.; Novoselov, K. S.; Geim, A. K.; Katsnelson, M. I.; Blake, P.; Morozov, S. V.; Schedin, F. Detection of Individual Gas Molecules Adsorbed on Graphene. *Nat. Mater.* **2007**, *6* (9), 652–655. https://doi.org/10.1038/nmat1967.

(7) Yuan, W.; Shi, G. Graphene-Based Gas Sensors. *J. Mater. Chem. A* **2013**, *1* (35), 10078. https://doi.org/10.1039/c3ta11774j.

(8) Sysoev, V.; Kolmakov, A.; Varezhnikov, A.; Lipatov, A.; Sinitskii, A.; Wilson, P. Highly Selective Gas Sensor Arrays Based on Thermally Reduced Graphene Oxide. *Nanoscale* **2013**, *5* (12), 5426. https://doi.org/10.1039/c3nr00747b.

(9) Kim, H. G.; Lee, H. B. R. Atomic Layer Deposition on 2D Materials. *Chem. Mater.* **2017**, *29* (9), 3809–3826. https://doi.org/10.1021/acs.chemmater.6b05103.

(10) Tutuc, E.; Colombo, L.; Nah, J.; Shahrjerdi, D.; Yao, Z.; Kim, S.; Jo, I.; Banerjee, S. K. Realization of a High Mobility Dual-Gated Graphene Field-Effect Transistor with Al2O3 Dielectric. *Appl. Phys. Lett.* **2009**, *94* (6), 062107. https://doi.org/10.1063/1.3077021.

(11) Vaziri, S.; Östling, M.; Lemme, M. C. A Hysteresis-Free High-k Dielectric and Contact Resistance Considerations for Graphene Field Effect Transistors. In *ECS Transactions*; The Electrochemical Society, 2011; Vol. 41, pp 165–171. https://doi.org/10.1149/1.3633296.

(12) Fallahazad, B.; Lee, K.; Lian, G.; Kim, S.; Corbet, C. M.; Ferrer, D. A.; Colombo, L.; Tutuc, E. Scaling of Al2O3dielectric for Graphene Field-Effect Transistors. *Appl. Phys. Lett.* **2012**, *100* (9), 10–14. https://doi.org/10.1063/1.3689785.

(13) Wang, X.; Tabakman, S. M.; Dai, H. Atomic Layer Deposition of Metal Oxides on Pristine and Functionalized Graphene. *J. Am. Chem. Soc.* **2008**, *130* (26), 8152–8153. https://doi.org/10.1021/ja8023059.

(14) Liu, R.; Peng, M.; Zhang, H.; Wan, X.; Shen, M. Atomic Layer Deposition of ZnO on Graphene for Thin Film Transistor. *Mater. Sci. Semicond. Process.* **2016**, *56*, 324–328. https://doi.org/10.1016/J.MSSP.2016.09.016.

(15) Nayfeh, O. M.; Marr, T.; Dubey, M. Impact of Plasma-Assisted Atomic-Layer-Deposited Gate Dielectric on Graphene Transistors. *IEEE Electron Device Lett.* **2011**, *32* (4), 473–475. https://doi.org/10.1109/LED.2011.2108258.

(16) Dimitrakopoulos, C.; Lin, Y.-M.; Grill, A.; Farmer, D. B.; Freitag, M.; Sun, Y.; Han, S.-J.; Chen, Z.; Jenkins, K. A.; Zhu, Y.; et al. Wafer-Scale Epitaxial Graphene Growth on the Si-Face of Hexagonal SiC (0001) for High Frequency Transistors. *J. Vac. Sci. Technol. B, Nanotechnol. Microelectron. Mater. Process. Meas. Phenom.* **2010**, *28* (5), 985–992. https://doi.org/10.1116/1.3480961.

(17) Zhang, X.; Schiros, T.; Nordlund, D.; Shin, Y. C.; Kong, J.; Dresselhaus, M.; Palacios, T. X-Ray Spectroscopic Investigation of Chlorinated Graphene: Surface Structure and Electronic Effects. *Adv. Funct. Mater.* **2015**. https://doi.org/10.1002/adfm.201500541.

(18) Zhang, X.; Hsu, A.; Wang, H.; Song, Y.; Kong, J.; Dresselhaus, M. S.; Palacios, T. Impact of Chlorine Functionalization on High-Mobility Chemical Vapor Deposition Grown Graphene. *ACS Nano* **2013**, *7* (8), 7262–7270. https://doi.org/10.1021/nn4026756.

(19) Li, B.; Zhou, L.; Wu, D.; Peng, H.; Yan, K.; Zhou, Y.; Liu, Z. Photochemical Chlorination of Graphene. In *ACS Nano*; 2011; Vol. 5, pp 5957–5961. https://doi.org/10.1021/nn201731t.

(20) Zhou, L.; Zhou, L.; Yang, M.; Wu, D.; Liao, L.; Yan, K.; Xie, Q.; Liu, Z.; Peng, H.; Liu, Z. Free Radical Reactions in Two Dimensions: A Case Study on Photochlorination of Graphene. *Small* **2013**, *9* (8), 1388–1396. https://doi.org/10.1002/smll.201202969.

(21) Tran, N. T. T.; Nguyen, D. K.; Glukhova, O. E.; Lin, M.-F. Coverage-Dependent Essential

Properties of Halogenated Graphene: A DFT Study. *Sci. Rep.* **2017**, *7* (1), 17858. https://doi.org/10.1038/s41598-017-18170-8.

(22) Hohenberg, P.; Kohn, W. Inhomogeneous Electron Gas. *Phys. Rev.* **1964**, *136*, B864--B871.

(23) Kohn, W.; Sham, L. J. Self-Consistent Equations Including Exchange and Correlation Effects. *Phys. Rev.* **1965**, *140*, A1133–A1138.

(24) Kresse, G.; Furthmüller, J. Efficiency of Ab-Initio Total Energy Calculations for Metals and Semiconductors Using a Plane-Wave Basis Set. *Comput. Mater. Sci.* **1996**, *6* (1), 15–50.

(25) Perdew, J. P.; Burke, K.; Ernzerhof, M. Generalized Gradient Approximation Made Simple. *Phys. Rev. Lett.* **1996**, *77* (18), 3865–3868. https://doi.org/10.1103/PhysRevLett.77.3865.

(26) Hannes Jónsson, Greg Mills and, K. W. J. Nudged Elastic Band Method for Finding Minimum Energy Paths of Transitions. In *Classical and Quantum Dynamics in Condensed Phase Simulations*; WORLD SCIENTIFIC, 1998; pp 385–404. https://doi.org/doi:10.1142/9789812839664_0016.

(27) Dresselhaus, M. S.; Jorio, A.; Cançado, L. G.; Dresselhaus, G.; Saito, R. Raman Spectroscopy: Characterization of Edges, Defects, and the Fermi Energy of Graphene and Sp 2 Carbons. *Nanosci. Technol.* **2012**. https://doi.org/10.1007/978-3-642-22984-8__2.

(28) Ferrari, A. C.; Basko, D. M. Raman Spectroscopy as a Versatile Tool for Studying the Properties of Graphene. *Nature Nanotechnology*. 2013. https://doi.org/10.1038/nnano.2013.46.